



THE UNIVERSITY *of* EDINBURGH

Edinburgh Research Explorer

## Formation and Stability of Dense Methane-Hydrogen Compounds

**Citation for published version:**

Ranieri, U, Conway, LJ, Donnelly, M-E, Hu, H, Wang, M, Dalladay-Simpson, P, Pena-Alvarez, M, Gregoryanz, E, Hermann, A & Howie, RT 2022, 'Formation and Stability of Dense Methane-Hydrogen Compounds', *Physical Review Letters*, vol. 128, no. 21, 215702, pp. 1-6.  
<https://doi.org/10.1103/PhysRevLett.128.215702>

**Digital Object Identifier (DOI):**

[10.1103/PhysRevLett.128.215702](https://doi.org/10.1103/PhysRevLett.128.215702)

**Link:**

[Link to publication record in Edinburgh Research Explorer](#)

**Document Version:**

Peer reviewed version

**Published In:**

Physical Review Letters

**General rights**

Copyright for the publications made accessible via the Edinburgh Research Explorer is retained by the author(s) and / or other copyright owners and it is a condition of accessing these publications that users recognise and abide by the legal requirements associated with these rights.

**Take down policy**

The University of Edinburgh has made every reasonable effort to ensure that Edinburgh Research Explorer content complies with UK legislation. If you believe that the public display of this file breaches copyright please contact [openaccess@ed.ac.uk](mailto:openaccess@ed.ac.uk) providing details, and we will remove access to the work immediately and investigate your claim.



## Important Notice to Authors

*No further publication processing will occur until we receive your response to this proof.*

Attached is a PDF proof of your forthcoming article in *Physical Review Letters*. The article accession code is LL17763. Your paper will be in the following section of the journal: LETTERS — Condensed Matter: Structure, etc.

Please note that as part of the production process, APS converts all articles, regardless of their original source, into standardized XML that in turn is used to create the PDF and online versions of the article as well as to populate third-party systems such as Portico, Crossref, and Web of Science. We share our authors' high expectations for the fidelity of the conversion into XML and for the accuracy and appearance of the final, formatted PDF. This process works exceptionally well for the vast majority of articles; however, please check carefully all key elements of your PDF proof, particularly any equations or tables.

Figures submitted electronically as separate files containing color appear in color in the online journal. However, all figures will appear as grayscale images in the print journal unless the color figure charges have been paid in advance, in accordance with our policy for color in print (<https://journals.aps.org/authors/color-figures-print>).

### Specific Questions and Comments to Address for This Paper


The numbered items below correspond to numbers in the margin of the proof pages pinpointing the source of the question and/or comment. The numbers will be removed from the margins prior to publication.

- 1 Please review the funding information section of the proof's cover letter and respond as appropriate. We must receive confirmation that the funding agencies have been properly identified before the article can publish.
- 2 This query was generated by an automatic reference checking system. References [18,25,56,59,62,63] could not be located in the databases used by the system. While the references may be correct, we ask that you check them so we can provide as many links to the referenced articles as possible.
- 3 NOTE: External links, which appear as blue text in the reference section, are created for any reference where a Digital Object Identifier (DOI) can be found. Please confirm that the links created in this PDF proof, which can be checked by clicking on the blue text, direct the reader to the correct references online. If there is an error, correct the information in the reference or supply the correct DOI for the reference. If no correction can be made or the correct DOI cannot be supplied, the link will be removed.
- 4 Please note that the references have been reordered so that they are cited in the text in numerical order.
- 5 Please check and confirm updated for Ref. [44].
- 6 Please note that Ref. [45] have been set up in the style used by APS for Supplemental Material references. The URL link will be activated at the time of publication.

### Titles in References

The editors now encourage insertion of article titles in references to journal articles and e-prints. This format is optional, but if chosen, authors should provide titles for *all* eligible references. If article titles remain missing from eligible references, the production team will remove the existing titles at final proof stage.

### ORCIDs

Please follow any ORCID links () after the authors' names and verify that they point to the appropriate record for each author.

### Crossref Funder Registry ID:

Information about an article's funding sources is now submitted to Crossref to help you comply with current or future funding agency mandates. Crossref's Funder Registry (<https://www.crossref.org/services/funder-registry/>) is the definitive registry of funding agencies. Please ensure that your acknowledgments include all sources of funding for your article following any requirements of your funding sources. Where possible, please include grant and award ids. Please carefully check the following funder information we have already extracted from your article and ensure its accuracy and completeness:

- European Synchrotron Radiation Facility, FundRef ID <http://dx.doi.org/10.13039/501100001671> (Republic of France/FR)
- H2020 European Research Council, FundRef ID <http://dx.doi.org/10.13039/100010663> (European Union/EU)
- Horizon 2020 Framework Programme, FundRef ID <http://dx.doi.org/10.13039/100010661> (European Union/EU)
- UK Research and Innovation, FundRef ID <http://dx.doi.org/10.13039/100014013> (United Kingdom of Great Britain and Northern Ireland/GB)
- United Kingdom Car-Parrinello consortium
- United Kingdom Materials and Molecular Modelling Hub

## Other Items to Check

- Please note that the original manuscript has been converted to XML prior to the creation of the PDF proof, as described above. Please carefully check all key elements of the paper, particularly the equations and tabular data.
- Title: Please check; be mindful that the title may have been changed during the peer-review process.
- Author list: Please make sure all authors are presented, in the appropriate order, and that all names are spelled correctly.
- Please make sure you have inserted a byline footnote containing the email address for the corresponding author, if desired. Please note that this is not inserted automatically by this journal.
- Affiliations: Please check to be sure the institution names are spelled correctly and attributed to the appropriate author(s).
- Receipt date: Please confirm accuracy.
- Acknowledgments: Please be sure to appropriately acknowledge all funding sources.
- References: Please check to ensure that titles are given as appropriate.
- Hyphenation: Please note hyphens may have been inserted in word pairs that function as adjectives when they occur before a noun, as in “x-ray diffraction,” “4-mm-long gas cell,” and “*R*-matrix theory.” However, hyphens are deleted from word pairs when they are not used as adjectives before nouns, as in “emission by x rays,” “was 4 mm in length,” and “the *R* matrix is tested.”  
Note also that Physical Review follows U.S. English guidelines in that hyphens are not used after prefixes or before suffixes: superresolution, quasiequilibrium, nanoprecipitates, resonancelike, clockwise.
- Please check that your figures are accurate and sized properly. Make sure all labeling is sufficiently legible. Figure quality in this proof is representative of the quality to be used in the online journal. To achieve manageable file size for online delivery, some compression and downsampling of figures may have occurred. Fine details may become somewhat fuzzy, especially in color figures. The print journal uses files of higher resolution and therefore details may be sharper in print. Figures to be published in color online will appear in color on these proofs if viewed on a color monitor or printed on a color printer.
- Overall, please proofread the entire *formatted* article very carefully. The redlined PDF should be used as a guide to see changes that were made during copyediting. However, note that some changes to math and/or layout may not be indicated.

## Ways to Respond

- **Web:** If you accessed this proof online, follow the instructions on the web page to submit corrections.

- **Email:** Send corrections to [aps-robot@luminad.com](mailto:aps-robot@luminad.com). Include the accession code LL17763 in the subject line.
- **Fax:** Return this proof with corrections to +1.855.808.3897.

### **If You Need to Call Us**

You may leave a voicemail message at +1.855.808.3897. Please reference the accession code and the first author of your article in your voicemail message. We will respond to you via email.

## Formation and Stability of Dense Methane-Hydrogen Compounds

Umbertoluca Ranieri<sup>1,2</sup>, Lewis Conway<sup>3</sup>, Mary-Ellen Donnelly<sup>1</sup>, Huixin Hu<sup>1</sup>, Mengnan Wang<sup>1</sup>, Philip Dalladay-Simpson<sup>1</sup>, Miriam Peña-Alvarez<sup>3</sup>, Eugene Gregoryanz<sup>1,3,4</sup>, Andreas Hermann<sup>3</sup>, and Ross T. Howie<sup>1,3,\*</sup>

<sup>1</sup>Center for High Pressure Science and Technology Advanced Research, 1690 Cailun Road, Shanghai, 201203, China

<sup>2</sup>Dipartimento di Fisica, Università di Roma La Sapienza, Piazzale Aldo Moro 5, 00185 Rome, Italy

<sup>3</sup>Centre for Science at Extreme Conditions and The School of Physics and Astronomy, The University of Edinburgh, Peter Guthrie Tait Road, Edinburgh, United Kingdom

<sup>4</sup>Key Laboratory of Materials Physics, Institute of Solid State Physics, CAS, Hefei, China

(Received 25 November 2021; revised 2 February 2022; accepted 20 April 2022)

Through a series of x-ray diffraction, optical spectroscopy diamond anvil cell experiments, combined with density functional theory calculations, we explore the dense CH<sub>4</sub>-H<sub>2</sub> system. We find that pressures as low as 4.8 GPa can stabilize CH<sub>4</sub>(H<sub>2</sub>)<sub>2</sub> and (CH<sub>4</sub>)<sub>2</sub>H<sub>2</sub>, with the latter exhibiting extreme hardening of the intramolecular vibrational mode of H<sub>2</sub> units within the structure. On further compression, a unique structural composition, (CH<sub>4</sub>)<sub>3</sub>(H<sub>2</sub>)<sub>25</sub>, emerges. This novel structure holds a vast amount of molecular hydrogen and represents the first compound to surpass 50 wt % H<sub>2</sub>. These compounds, stabilized by nuclear quantum effects, persist over a broad pressure regime, exceeding 160 GPa.

DOI:

Hydrogen and methane are, besides water, the most prevalent small molecules in the outer Solar System. Their interplay under extreme conditions is of key interest to understanding the evolution and interior dynamics of Neptune and Uranus, as well as of Earth and exoplanets [1–4]. The simplest molecule, H<sub>2</sub>, has been shown to exhibit rich physical phenomena, including quantum rotational phases and pressure-induced steps toward an atomic metallic solid, while methane (CH<sub>4</sub>), the simplest hydrocarbon, has been proposed to polymerize during compression to form long-chain hydrocarbons and at further extremes decompose into diamond plus H<sub>2</sub> [5–19].

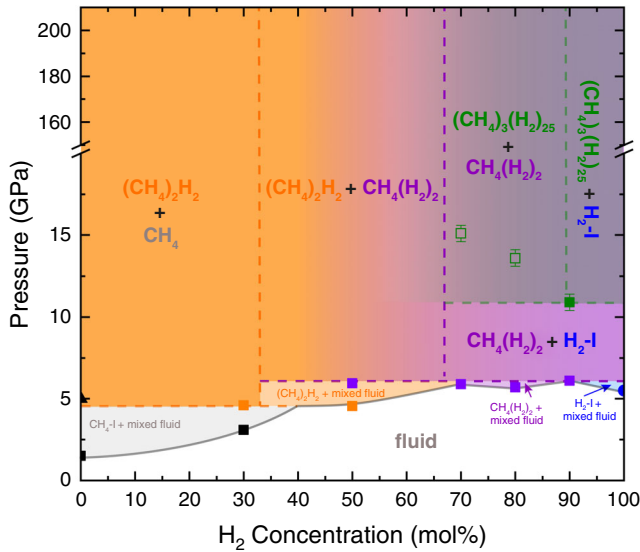
Hydrogen reacts with a number of materials at high pressures and temperatures but also has a propensity to form van der Waals compounds that can be stable far beyond 100 GPa [20–32]. Methane and hydrogen were first reported to crystallize into inclusion (host-guest) compounds over 25 years ago at pressures between 5 and 7 GPa. A range of compositions were claimed: (CH<sub>4</sub>)<sub>2</sub>H<sub>2</sub>, CH<sub>4</sub>H<sub>2</sub>, CH<sub>4</sub>(H<sub>2</sub>)<sub>2</sub>, and CH<sub>4</sub>(H<sub>2</sub>)<sub>4</sub> [21]. However, the experimental evidence for these compounds was limited, with only the shift of the hydrogen intramolecular vibrational mode  $\nu_1$ -H<sub>2</sub> (vibron) relative to that of pure hydrogen being reported together with the lattice parameters of potential structures. Assuming that these structural compositions were correct, a later experimental study explored the recoverability of CH<sub>4</sub>(H<sub>2</sub>)<sub>4</sub> at low temperature to investigate its potential as a hydrogen storage media [33,34].

In contrast to experimental work, the CH<sub>4</sub>-H<sub>2</sub> system has recently had a surge of theoretical investigations, predicting a variety of extremely hydrogen-rich compositions to emerge such as triclinic (CH<sub>4</sub>)<sub>2</sub>(H<sub>2</sub>)<sub>3</sub>, trigonal (CH<sub>4</sub>)<sub>2</sub>(H<sub>2</sub>)<sub>7</sub>, and

hexagonal CH<sub>4</sub>(H<sub>2</sub>)<sub>9</sub>, as well as several CH<sub>4</sub>H<sub>2</sub> structures [18,35–37]. Furthermore, it was suggested that CH<sub>4</sub>-H<sub>2</sub> structures could be the most stable form of carbon and hydrogen at pressures up to 200 GPa [18].

Surprisingly, given these predictions and the advent of technological advances over the past 25 years, no further experimental exploration has been conducted despite undetermined CH<sub>4</sub>-H<sub>2</sub> compound signatures emerging as a by-product in many prolific studies of hydrocarbons at planetary conditions [3,19,38–41]. Moreover, the doping of carbon (or methane) could even enhance the properties of materials at extreme pressures, with the unprecedented claim of room temperature superconductivity in the carbonaceous sulfur hydride system [42–44]. The lack of knowledge regarding CH<sub>4</sub>-H<sub>2</sub> compound formation inhibits our understanding of these more complex ternary systems and how doping could induce novel properties. As such, it is of fundamental interest to know which methane-hydrogen compounds are actually formed and test their pressure stability limits.

In this Letter, we have conducted a series of high-pressure synchrotron powder x-ray diffraction and Raman spectroscopy experiments in diamond anvil cells combined with density functional theory (DFT) calculations and structural searching to explore the formation and properties of CH<sub>4</sub>-H<sub>2</sub> compounds from mixtures of methane and hydrogen. In H<sub>2</sub>-rich mixtures, we observe the formation of hexagonal CH<sub>4</sub>(H<sub>2</sub>)<sub>2</sub> above 5 GPa, before partially transforming into monoclinic (CH<sub>4</sub>)<sub>3</sub>(H<sub>2</sub>)<sub>25</sub>. (CH<sub>4</sub>)<sub>3</sub>(H<sub>2</sub>)<sub>25</sub> represents a unique composition and contains an unprecedented 51.1 wt % H<sub>2</sub>, which is the highest hydrogen content of any currently known



F1:1 FIG. 1. Pressure-composition phase diagram of the  $\text{CH}_4\text{-H}_2$   
 F1:2 binary system. Filled square symbols indicate the formation  
 F1:3 pressures of each compound:  $(\text{CH}_4)_2\text{H}_2$  (orange),  $\text{CH}_4(\text{H}_2)_2$   
 F1:4 (purple), and  $(\text{CH}_4)_3(\text{H}_2)_{25}$  (green). The green open squares  
 F1:5 represent the pressures at which  $(\text{CH}_4)_3(\text{H}_2)_{25}$  is first observed.  
 F1:6 The black squares, black triangle, and blue circle represent  
 F1:7 the formation pressure of  $\text{CH}_4\text{-I}$ ,  $\text{CH}_4\text{-A}$ , and  $\text{H}_2\text{-I}$ , respectively.  
 F1:8 The gray line represents the liquidus curve and is adapted from  
 F1:9 Ref. [21]. Below 7 GPa, the error in pressure is  $\pm 0.2$  GPa and  
 F1:10 smaller than the size of the symbol. Initial gas mixtures have a  
 F1:11 tolerance of 1%.

83 stoichiometric compound. In  $\text{CH}_4$ -rich mixtures, tetrago-  
 84 nal  $(\text{CH}_4)_2\text{H}_2$  forms, which undergoes extreme hardening  
 85 of the  $\text{H}_2$  intramolecular vibrational mode with pressure.  
 86 All three compounds exhibit remarkable stability, exceed-  
 87 ing pressures of 160 GPa.

88 At pressures below 1.5 GPa, all mixture concentrations  
 89 (30, 50, 70, 80, and 90 mol %  $\text{H}_2$ ) are homogeneous well-  
 90 mixed fluids and display the Raman signatures of both  
 91 constituent species (see Fig. 1 for the pressure-composition  
 92 phase diagram, Supplemental Material [45] for experimental  
 93 methods, and Figs. S1–S9 [45] for Raman spectra of all  
 94 mixtures). On compression of hydrogen-rich  $\text{CH}_4\text{-H}_2$  mix-  
 95 tures (50–90 mol %  $\text{H}_2$ ) above 5 GPa, the fluid mixture  
 96 crystallizes into a solid which we identify as  $\text{CH}_4(\text{H}_2)_2$ .  
 97 X-ray diffraction measurements reveal that this compound  
 98 adopts a hexagonal  $\text{MgZn}_2$  Laves phase structure (space  
 99 group  $P6_3/mmc$ ), where the  $\text{CH}_4$  molecules occupy the Mg  
 100 sites and the  $\text{H}_2$  molecules occupy the Zn sites (see Fig. 2),  
 101 the lattice parameters of which are  $a = 4.981 \text{ \AA}$  and  
 102  $c = 8.125 \text{ \AA}$  at 16.6 GPa. This structure and composition  
 103 was suggested previously but attributed to a compound  
 104 forming in a narrow pressure regime (between approxi-  
 105 mately 6 and 7 GPa) and between 35 and 65 mol %  $\text{H}_2$   
 106 mixture concentrations [21]. Here, we find that  $\text{CH}_4(\text{H}_2)_2$  is  
 107 the dominant phase across all  $\text{H}_2$ -rich mixtures and persis-  
 108 tent over a large pressure regime. Raman spectroscopy

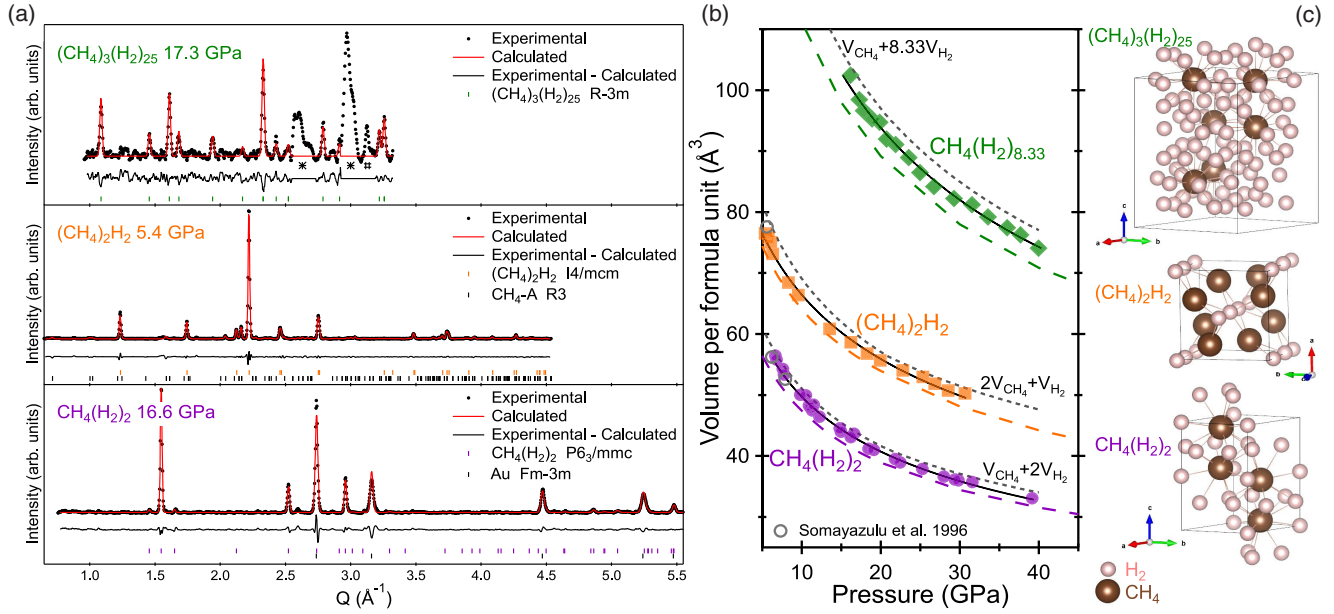
109 reveals two distinct  $\text{H}_2$  vibrons,  $\nu_{1H}$  and  $\nu_{2H}$ , the latter  
 110 of which is approximately 50 times lower in intensity.  
 111 The two most intense  $\text{CH}_4$  stretching modes,  $\nu_{1M}$  and  $\nu_{2M}$ ,  
 112 are shifted to higher frequency compared to pure  $\text{CH}_4$ ,  
 113 while the wagging mode is shifted to lower frequency  
 114 (see Figs. 3 and 4).

115 On further compression, we observe another compound  
 116 emerge evidenced by visual changes in the sample mor-  
 117 phology and the appearance of three distinct  $\text{H}_2$  vibra-  
 118 tional modes (the lowest in frequency being the most intense by 2  
 119 orders of magnitude) and  $\text{CH}_4$  stretching bands that can be  
 120 isolated from  $\text{CH}_4(\text{H}_2)_2$  (see Figs. 3 and 4 and Supplemental  
 121 Material [45]). The most intense  $\text{H}_2$  vibron is lower in  
 122 frequency than that of  $\text{CH}_4(\text{H}_2)_2$ , suggestive that the  
 123 compound has a higher  $\text{H}_2$  content. X-ray diffraction  
 124 measurements indicate the compound is weakly scattering;  
 125 however, this could be in part due to only partial trans-  
 126 formation of the sample. The patterns could be indexed to a  
 127 hexagonal cell, with  $a = 7.804 \text{ \AA}$  and  $c = 11.199 \text{ \AA}$  at  
 128 17.3 GPa (see Fig. 2). Systematic absences, unit cell volume,  
 129 and  $c/a$  ratio suggest this compound has a close resem-  
 130 blance with the previously reported  $R\text{-}3m$  structure of  
 131  $\text{Xe}(\text{H}_2)_8$  [23,26] and an initial composition estimate of  
 132  $\text{CH}_4(\text{H}_2)_8$ . This seemed plausible given  $\text{CH}_4$  and Xe have  
 133 similar van der Waals diameters (3.78 and 4.32  $\text{ \AA}$ ,  
 134 respectively).

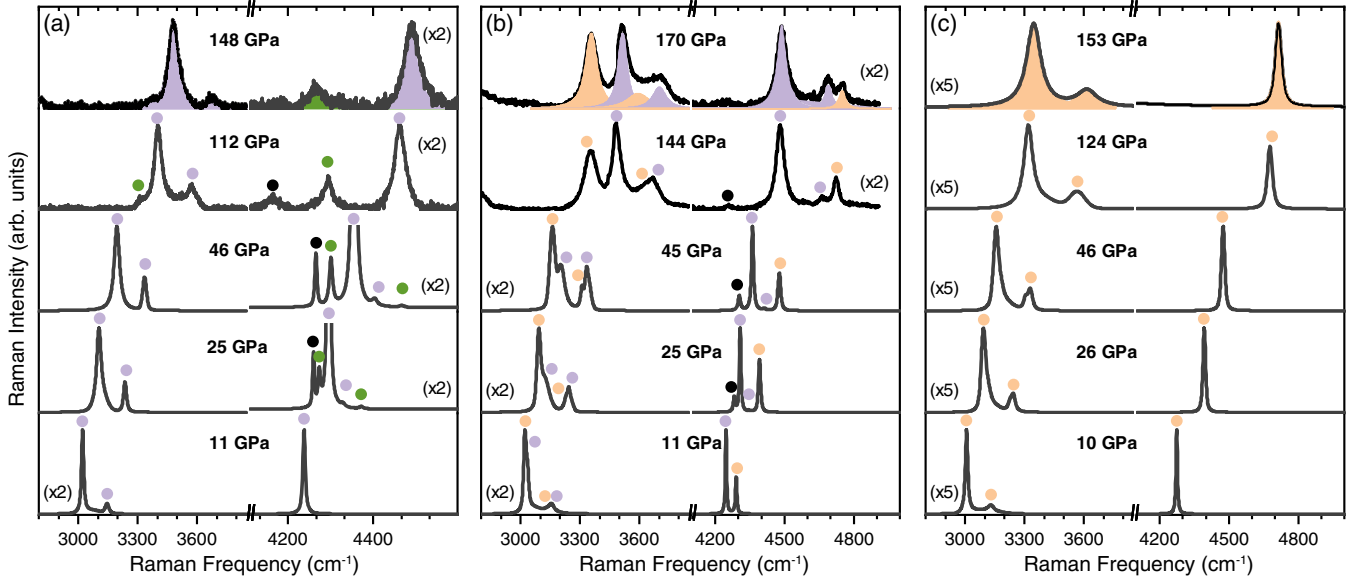
135 We subsequently performed DFT calculations to help  
 136 identify this phase. We constructed a series of structures of  
 137 variable composition, starting by populating the hexago-  
 138 nal cell with randomly oriented  $\text{CH}_4$  molecules on the Xe  
 139 sites of  $\text{Xe}(\text{H}_2)_8$ , before adding  $\text{H}_2$  molecules on hex-  
 140 agonal close packed (hcp) arrangements commensurate  
 141 with the cell, using up to  $3 \times 3 \times 4$  repeats of the hcp  
 142 lattice and a random offset against the  $\text{CH}_4$  sublattice.  $\text{H}_2$   
 143 molecules too close to  $\text{CH}_4$  were removed before fully  
 144 optimizing the remaining atoms and all lattice parameters.  
 145 Several thousand of these structures were generated with  
 146 stoichiometries ranging from  $\text{CH}_4(\text{H}_2)_7$  to  $\text{CH}_4(\text{H}_2)_{11}$ .  
 147 Of these,  $\text{CH}_4(\text{H}_2)_{8.33}$  [or  $(\text{CH}_4)_3(\text{H}_2)_{25}$ ] emerged as the  
 148 most energetically competitive and was found to be  
 149 dynamically stable at and above 20 GPa (see Figs. S19  
 150 and S20 [45]). It is also the only computationally obtained  
 151 structure which reproduces the positions and intensities of  
 152 the experimental diffraction peaks across the studied  
 153 pressure range (see Fig. S14 [45]), which is meaningful  
 154 given that no symmetry restrictions were applied in the  
 155 structures' construction and subsequent optimization. While  
 156 we find both  $\text{CH}_4(\text{H}_2)_2$  and  $(\text{CH}_4)_2\text{H}_2$  stable or close to  
 157 stability within the  $\text{CH}_4\text{-H}_2$  phase diagram across a wide  
 158 pressure range, once zero point energies and vibrational  
 159 entropies are accounted for,  $(\text{CH}_4)_3(\text{H}_2)_{25}$  remains meta-  
 160 stable throughout (see Supplemental Material [45]).

161 Considering methane and hydrogen molecules to be  
 162 spherical, the structure of  $(\text{CH}_4)_3(\text{H}_2)_{25}$  is monoclinic with  
 163 space group  $C2/m$  (coordinates are given in Supplemental

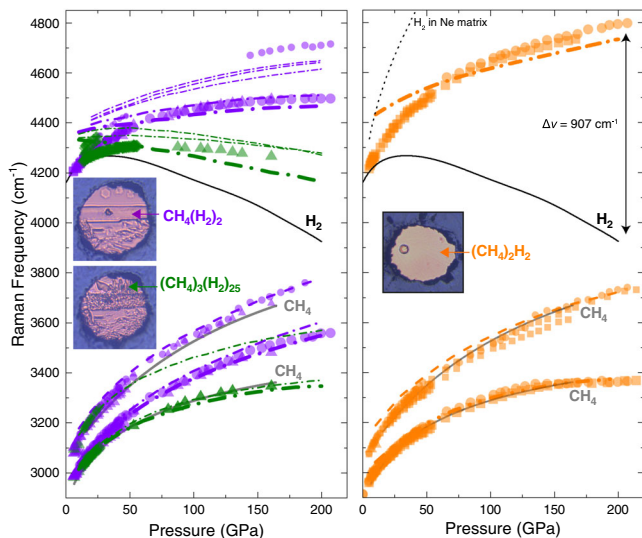




F2:1 FIG. 2. (a) Representative x-ray diffraction patterns of the three compounds plotted as a function of exchanged wave vector and their  
 F2:2 Le Bail refinements. Refinements include  $(\text{CH}_4)_3(\text{H}_2)_{25}$ - $R-3m$  ( $a = 7.804 \text{ \AA}$  and  $c = 11.199 \text{ \AA}$ ),  $(\text{CH}_4)_2\text{H}_2$ - $I4/mcm$  ( $a = 7.195 \text{ \AA}$   
 F2:3 and  $c = 5.909 \text{ \AA}$ ),  $\text{CH}_4$ - $A$ - $R3$  ( $a = 12.306 \text{ \AA}$  and  $c = 15.520 \text{ \AA}$ ),  $\text{CH}_4(\text{H}_2)_2$ - $P6_3/mmc$  ( $a = 4.981 \text{ \AA}$  and  $c = 8.125 \text{ \AA}$ ), and  
 F2:4  $\text{Au-Fm-}3m$  ( $a = 3.976 \text{ \AA}$ ). Excluded regions in the pattern of  $(\text{CH}_4)_3(\text{H}_2)_{25}$  correspond to rhenium (gasket material) and rhenium  
 F2:5 hydride (\*) and excess  $\text{H}_2$  (#). (b) Volumes per formula unit as a function of pressure. Symbols represent experimental data (the error  
 F2:6 bars are smaller than the symbol size), and black full lines represent their best second-order Birch-Murnaghan fits:  $\text{CH}_4(\text{H}_2)_{8.33}$ ,  
 F2:7  $V_0 = 246 \pm 17 \text{ \AA}^3$  and  $K = 3.0 \pm 0.6 \text{ GPa}$ ;  $(\text{CH}_4)_2\text{H}_2$ ,  $V_0 = 101 \pm 2 \text{ \AA}^3$  and  $K = 10.2 \pm 0.8 \text{ GPa}$ ;  $\text{CH}_4(\text{H}_2)_2$ ,  $V_0 = 90 \pm 3 \text{ \AA}^3$  and  
 F2:8  $K = 5.0 \pm 0.4 \text{ GPa}$ . Dashed lines represent volumes derived from our DFT calculations, and gray dotted lines represent the volumes of  
 F2:9 ideal mixtures of  $\text{CH}_4$ - $A$ / $\text{CH}_4$ - $B$  and  $\text{H}_2$ - $I$  using the previously determined equations of state [14,17,69]. The experimental volumes  
 F2:10 given in Ref. [21] are represented by gray circles. (c) Structural models of the three compounds, where  $\text{CH}_4$  and  $\text{H}_2$  are represented by  
 F2:11 brown and white spheres, respectively, and lines indicate  $\text{CH}_4$ - $\text{H}_2$  nearest neighbors.



F3:1 FIG. 3. Representative vibrational Raman spectra of (a) 70%  $\text{H}_2$ , (b) 50%  $\text{H}_2$ , and (c) 30%  $\text{H}_2$  mixtures. Colors indicate the modes  
 F3:2 assigned to  $\text{CH}_4(\text{H}_2)_2$  (purple),  $(\text{CH}_4)_3(\text{H}_2)_{25}$  (green),  $(\text{CH}_4)_2\text{H}_2$  (orange), and excess  $\text{H}_2$  (black).



F4:1 FIG. 4. Raman shift as a function of pressure of the H<sub>2</sub>  
 F4:2 vibrational modes and C-H stretching modes of CH<sub>4</sub>(H<sub>2</sub>)<sub>2</sub> and  
 F4:3 (CH<sub>4</sub>)<sub>3</sub>(H<sub>2</sub>)<sub>25</sub> (left panel, purple and green symbols, respec-  
 F4:4 tively), and (CH<sub>4</sub>)<sub>2</sub>H<sub>2</sub> (right panel, orange symbols). Frequencies  
 F4:5 are collated from 30% (squares), 50% (circles), 70% (triangles),  
 F4:6 80% (diamonds), and 90% (hexagons) H<sub>2</sub> mixtures, with the  
 F4:7 most intense modes represented by larger symbols. Raman  
 F4:8 frequencies of individual mixtures are given in Supplemental  
 F4:9 Material [45]. The dot-dashed lines represent the calculated  
 F4:10 frequencies of the H<sub>2</sub> modes and C-H stretching bands of each  
 F4:11 compound, with the thickest line representing the most intense  
 F4:12 modes. Black and gray solid lines represent pure H<sub>2</sub> [6] and CH<sub>4</sub>  
 F4:13 [15], respectively. The black dotted line represents the frequency  
 F4:14 of H<sub>2</sub> in a Ne matrix [70]. The error in pressure ranges from ±0.2  
 F4:15 below 50 GPa, ±1 below 150 GPa, and ±5 above. The error bars  
 F4:16 in frequency are smaller than the symbol size. Photomicrographs  
 F4:17 show examples of morphology of synthesised samples within the  
 F4:18 DAC sample chamber.

164 Material [45]). Le Bail refinements of the experimental  
 165 diffraction patterns were performed using the trigonal space  
 166 group  $R\bar{3}m$ , which is obtained considering the carbon atoms  
 167 only, and the hexagonal setting, which resulted in good fits  
 168 to the data. The obtained volume per methane molecule is  
 169 close to  $V_{\text{CH}_4} + 8.33V_{\text{H}_2}$  (see Fig. 2), the volume of an ideal  
 170 mixture of CH<sub>4</sub> and H<sub>2</sub> with the same composition. A  
 171 comparison between the experimental and computational  
 172 vibrational Raman modes of CH<sub>4</sub>(H<sub>2</sub>)<sub>2</sub>- $P6_3/mmc$  and  
 173 (CH<sub>4</sub>)<sub>3</sub>(H<sub>2</sub>)<sub>25</sub>- $C2/m$  is given in Fig. 4, where we see  
 174 qualitatively good agreement between the number of modes,  
 175 relative intensity, and frequency for both compounds.

176 In methane-rich concentrations of 30 mol% H<sub>2</sub>, we  
 177 observe a body-centered tetragonal Al<sub>2</sub>Cu-type structure  
 178 (space group  $I4/mcm$ ) to form above 4.6 GPa (with  $a =$   
 179  $7.195 \text{ \AA}$  and  $c = 5.909 \text{ \AA}$  at 5.4 GPa), which is consistent  
 180 with the previously reported composition of (CH<sub>4</sub>)<sub>2</sub>H<sub>2</sub> [21]  
 181 (see Fig. 1). Raman spectroscopy measurements show that  
 182 the CH<sub>4</sub> stretching bands of (CH<sub>4</sub>)<sub>2</sub>H<sub>2</sub> are close to the  
 183 frequencies of pure solid CH<sub>4</sub>, while two wagging modes are

184 observed. The number of modes and frequencies are in good  
 185 agreement with our calculated values (see Fig. 4). The  $\nu_{1H}$   
 186 mode, corresponding to H<sub>2</sub> units within the structure,  
 187 exhibits the most extreme hardening of any stoichiometric  
 188 molecular compound [25,28]. At a pressure of 207 GPa,  
 189 (CH<sub>4</sub>)<sub>2</sub>H<sub>2</sub>- $\nu_{1H}$  has a frequency of 4798 cm<sup>-1</sup>, over  
 190 900 cm<sup>-1</sup> higher than H<sub>2</sub>- $\nu_1$  (see Fig. 4). Remarkably, the  
 191 frequencies we observe reach similar values to an impurity  
 192 H<sub>2</sub> molecule isolated in a noble gas matrix, albeit at higher  
 193 pressure [70]. Up to pressures of 207 GPa, we do not observe  
 194 a turnover of  $\nu_{1H}$  (and 500 GPa in our calculations), unlike in  
 195 pure H<sub>2</sub>, which exhibits a maximum frequency at approx-  
 196 imately 38 GPa [5].

197 These results highlight the enormous impact that the  
 198 local environment around a H<sub>2</sub> molecule can have on its  
 199 vibron frequency. In Supplemental Material [45], we  
 200 present a simple molecular model demonstrating that the  
 201 vibron frequency of a H<sub>2</sub> surrounded by two CH<sub>4</sub>  
 202 (respectively, H<sub>2</sub>) will continuously increase (respectively,  
 203 decrease) if the surrounding molecules are pushed closer.  
 204 A molecular orbital analysis reveals that, in H<sub>2</sub>-dominated  
 205 environments, intermolecular interactions lead to occu-  
 206 pancy of antibonding H-H  $\sigma^*$  states, which does not  
 207 happen in CH<sub>4</sub>-dominated environments. In (CH<sub>4</sub>)<sub>2</sub>H<sub>2</sub>,  
 208 every H<sub>2</sub> has two nearest H<sub>2</sub> neighbors and eight nearest  
 209 CH<sub>4</sub> neighbors; as a result, the vibron exhibits extreme  
 210 hardening [see Fig. 2(c) and Supplemental Material [45]  
 211 for graphical representations of the unit cells and inter-  
 212 molecular distances]. This local environment is reversed  
 213 in (CH<sub>4</sub>)<sub>3</sub>(H<sub>2</sub>)<sub>25</sub> with an average of 9.8 H<sub>2</sub> neighbors but  
 214 only 2.24 CH<sub>4</sub> neighbors per H<sub>2</sub> molecule; still, it remains  
 215 very different from H<sub>2</sub>-I, having a coordination number of  
 216 12 and considerably shorter H<sub>2</sub>-H<sub>2</sub> distances [28]. For  
 217 (CH<sub>4</sub>)<sub>3</sub>(H<sub>2</sub>)<sub>25</sub>, the  $\nu_{1H}$  mode has a maximum at about  
 218 70 GPa, and the vibron frequencies tend toward the values  
 219 found for pure H<sub>2</sub>. In CH<sub>4</sub>(H<sub>2</sub>)<sub>2</sub>, where each H<sub>2</sub> has six  
 220 nearest H<sub>2</sub> neighbors and six nearest CH<sub>4</sub> neighbors, the  
 221 vibron frequencies are interpolated between (CH<sub>4</sub>)<sub>3</sub>(H<sub>2</sub>)<sub>25</sub>  
 222 and (CH<sub>4</sub>)<sub>2</sub>H<sub>2</sub>.

223 We find that the pressure-composition phase diagram is  
 224 simpler than previously reported [21], with only three  
 225 stable CH<sub>4</sub>-H<sub>2</sub> compositions. In 50 mol% H<sub>2</sub> mixtures,  
 226 we observe the coexistence of both (CH<sub>4</sub>)<sub>2</sub>H<sub>2</sub> and  
 227 CH<sub>4</sub>(H<sub>2</sub>)<sub>2</sub>, together with some excess H<sub>2</sub>, indicative that  
 228 equilibrium has not been reached. Furthermore, we observe  
 229 trace amounts of (CH<sub>4</sub>)<sub>3</sub>(H<sub>2</sub>)<sub>25</sub>, which can be attributed to  
 230 macroscopic inhomogeneity within the sample chamber. In  
 231 70 mol% mixtures and 80 mol% H<sub>2</sub> mixtures, we first  
 232 observe the Raman signatures of (CH<sub>4</sub>)<sub>3</sub>(H<sub>2</sub>)<sub>25</sub> at 14.5 GPa  
 233 and in 13.6 GPa (shown as open symbols in Fig. 1),  
 234 respectively, while in 90 mol% mixtures, we observe  
 235 (CH<sub>4</sub>)<sub>3</sub>(H<sub>2</sub>)<sub>25</sub> at 10.9 GPa. It is possible that, in 70 mol  
 236 % mixtures and 80 mol% H<sub>2</sub> mixtures, formation occurs at  
 237 lower pressure but is below the detection limit in the Raman  
 238 spectra. We find that even in 90 mol% mixtures the



239 transformation from  $\text{CH}_4(\text{H}_2)_2$  and  $\text{H}_2$  to  $(\text{CH}_4)_3(\text{H}_2)_{25}$  is  
 240 never complete, suggestive that the transformation is  
 241 kinetically sluggish and due to hindered diffusion of  $\text{H}_2$   
 242 in the solid state. Although our liquidus curve is in good  
 243 agreement with that reported previously, we do not observe  
 244 either  $\text{CH}_4\text{H}_2$  and  $\text{CH}_4(\text{H}_2)_4$  and attribute this to a mis-  
 245 interpretation of  $\text{CH}_4(\text{H}_2)_2$  [21]. The experimental volume  
 246 given for hexagonal wurtzite  $\text{CH}_4\text{H}_2$  is identical to our  
 247 experimental volume for  $\text{CH}_4(\text{H}_2)_2$  at the same given  
 248 pressure. Furthermore, after extensive structure searches,  
 249 with randomly orientated molecules in the reported wurt-  
 250 zite center-of-mass positions, we do not find any version of  
 251 the hexagonal wurtzite structure to be dynamically stable.  
 252 The evidence for  $\text{CH}_4(\text{H}_2)_4$  was predominantly based on  
 253 Raman spectroscopy, and we find to be a misinterpretation  
 254 of the coexistence between the  $\text{CH}_4\text{-H}_2$  mixed fluid and  
 255 solid  $\text{CH}_4(\text{H}_2)_2$  (see Fig. S8 [45]).

256  $(\text{CH}_4)_3(\text{H}_2)_{25}$  possesses 51.1 wt % molecular hydrogen  
 257 (63.4 wt % if the hydrogen of methane is included), which is  
 258 the highest hydrogen content of any currently known  
 259 stoichiometric compound. Notwithstanding the good agree-  
 260 ment between the experimental and calculated data,  
 261  $(\text{CH}_4)_3(\text{H}_2)_{25}$  represents an unusual and unique composi-  
 262 tion. All three compounds exhibit remarkable stability, with  
 263 the Raman signatures of  $(\text{CH}_4)_2\text{H}_2$  and  $\text{CH}_4(\text{H}_2)_2$  detect-  
 264 able to at least 215 GPa and  $(\text{CH}_4)_3(\text{H}_2)_{25}$  up to 165 GPa.  
 265 We estimate the melting temperatures  $T_m$  of  $(\text{CH}_4)_2\text{H}_2$  and  
 266  $\text{CH}_4(\text{H}_2)_2$  using Lindemann’s equation based on calculated  
 267 Debye temperatures and found  $T_m$  significantly higher than  
 268 molecular hydrogen at all pressures (see Supplemental  
 269 Material [45]). This would imply that hydrogen mixed with  
 270 methane would potentially not possess the melting line  
 271 turnover that is observed in pure hydrogen [7]. Taken  
 272 together in a planetary context, this could influence critical  
 273 properties of planetary matter such as thermal conductivities  
 274 and viscosities. In a materials science context, high Debye  
 275 temperatures coupled with extremely large vibron frequen-  
 276 cies  $\nu_H$  are promising ingredients for high- $T_c$  superconduc-  
 277 tivity—provided a reasonable density of states  $N(E_F)$  at the  
 278 Fermi energy. The molecular compounds described here are  
 279 insulators (all remain transparent in the visible up to the  
 280 highest pressures reached), but the presence of an electron or  
 281 hole dopant would metallize the system, with partially  
 282 charged entities  $\text{H}_2^{\pm\delta}$  present. This motif, at least in calcu-  
 283 lations, can lead to  $T_c$  close to 200 K [71].

284 **1** Parts of this research were carried out at P02.2 at DESY, a  
 285 member of the Helmholtz Association (HGF), and we thank  
 286 H.-P. Liermann and K. Glazyrin for assistance. We also  
 287 acknowledge the European Synchrotron Radiation Facility  
 288 for provision of synchrotron radiation facilities at the ID15B  
 289 beam line and assistance from M. Hanfland and D.  
 290 Comboni. R. T. H. acknowledges that the project has  
 291 received funding from the European Research Council  
 292 (ERC) under the European Union’s Horizon 2020 research  
 293 and innovation program (Grant Agreement No. 948895

“MetElOne”). M. P.-A. acknowledges the support of the  
 European Research Council (ERC) Grant “Hecate” reference  
 No. 695527 and the UKRI Future leaders fellowship Mrc-  
 Mr/T043733/1. Computational resources provided by the  
 United Kingdom’s National Supercomputer Service through  
 the United Kingdom Car-Parrinello consortium (EP/  
 P022561/1) and Project ID No. d56 “Planetary Interiors”  
 and by the United Kingdom Materials and Molecular  
 Modelling Hub (EP/P020194) are gratefully acknowledged.  
 The authors thank J. Binns for useful discussions.

\*ross.howie@hpcstar.ac.cn

- [1] W. B. Hubbard, W. J. Nellis, A. C. Mitchell, N. C. Holmes, S. S. Limaye, and P. C. McCandless, *Science* **253**, 648 (1991). 2 308
- [2] R. Chau, S. Hamel, and W. J. Nellis, *Nat. Commun.* **2**, 203 (2011). 3 310
- [3] S. S. Lobanov, P.-N. Chen, X.-J. Chen, C.-S. Zha, K. D. Litasov, H.-K. Mao, and A. F. Goncharov, *Nat. Commun.* **4**, 2446 (2013). 4 311
- [4] R. Helled and J. J. Fortney, *Phil. Trans. R. Soc. A* **378**, 20190474 (2020). 312
- [5] H.-k. Mao and R. J. Hemley, *Rev. Mod. Phys.* **66**, 671 (1994). 313
- [6] R. T. Howie, C. L. Guillaume, T. Scheler, A. F. Goncharov, and E. Gregoryanz, *Phys. Rev. Lett.* **108**, 125501 (2012). 314
- [7] R. T. Howie, P. Dalladay-Simpson, and E. Gregoryanz, *Nat. Mater.* **14**, 495 (2015). 315
- [8] P. Dalladay-Simpson, R. T. Howie, and E. Gregoryanz, *Nature (London)* **529**, 63 (2016). 316
- [9] E. Gregoryanz, C. Ji, P. Dalladay-Simpson, B. Li, R. T. Howie, and H.-K. Mao, *Matter Radiat. Extremes* **5**, 038101 (2020). 317
- [10] P. Loubeyre, F. Occelli, and P. Dumas, *Nature (London)* **577**, 631 (2020). 318
- [11] R. M. Hazen, H.-K. Mao, L. W. Finger, and P. M. Bell, *Appl. Phys. Lett.* **37**, 288 (1980). 319
- [12] H. Hirai, K. Konagai, T. Kawamura, Y. Yamamoto, and T. Yagi, *Phys. Earth Planet. Inter.* **174**, 242 (2009). 320
- [13] L. Sun, A. L. Ruoff, C.-S. Zha, and G. Stupian, *J. Phys. Chem. Solids* **67**, 2603 (2006). 321
- [14] L. Sun, W. Yi, L. Wang, J. Shu, S. Sinogeikin, Y. Meng, G. Shen, L. Bai, Y. Li, J. Liu, H.-K. Mao, and W. L. Mao, *Chem. Phys. Lett.* **473**, 72 (2009). 322
- [15] J. E. Proctor, H. E. Maynard-Casely, M. A. Hakeem, and D. Cantiah, *J. Raman Spectrosc.* **48**, 1777 (2017). 323
- [16] H. E. Maynard-Casely, C. L. Bull, M. Guthrie, I. Loa, M. I. McMahon, E. Gregoryanz, R. J. Nelmes, and J. S. Loveday, *J. Chem. Phys.* **133**, 064504 (2010). 324
- [17] H. E. Maynard-Casely, L. F. Lundegaard, I. Loa, M. I. McMahon, E. Gregoryanz, R. J. Nelmes, and J. S. Loveday, *J. Chem. Phys.* **141**, 234313 (2014). 325
- [18] L. J. Conway and A. Hermann, *Geosciences bulletin Series A* **9**, 227 (2019). 326
- [19] M. Peña-Alvarez, A. V. Brovarone, M.-E. Donnelly, M. Wang, P. Dalladay-Simpson, R. Howie, and E. Gregoryanz, *Nat. Commun.* **12**, 6387 (2021). 327

- 353 [20] P. Loubeyre, R. Letoullec, and J.-P. Pinceaux, *Phys. Rev. Lett.* **72**, 1360 (1994). 413
- 354 414
- 355 [21] M. S. Somayazulu, L. W. Finger, R. J. Hemley, and H. K. Mao, *Science* **271**, 1400 (1996). 415
- 356 416
- 357 [22] T. A. Strobel, P. Ganesh, M. Somayazulu, P. R. C. Kent, and R. J. Hemley, *Phys. Rev. Lett.* **107**, 255503 (2011). 417
- 358 418
- 359 [23] M. Somayazulu, P. Dera, A. F. Goncharov, S. A. Gramsch, P. Liermann, W. Yang, Z. Liu, H.-K. Mao, and R. J. Hemley, *Nat. Chem.* **2**, 50 (2010). 419
- 360 420
- 361 421
- 362 [24] D. K. Spaulding, G. Weck, P. Loubeyre, F. Datchi, P. Dumas, and M. Hanfland, *Nat. Commun.* **5**, 5739 (2014). 422
- 363 423
- 364 [25] A. K. Kleppe, M. Amboage, and A. P. Jephcoat, *Sci. Rep.* **4**, 1 (2014). 424
- 365 425
- 366 [26] M. Somayazulu, P. Dera, J. Smith, and R. J. Hemley, *J. Chem. Phys.* **142**, 104503 (2015). 426
- 367 427
- 368 [27] E. J. Pace, J. Binns, M. Peña Alvarez, P. Dalladay-Simpson, E. Gregoryanz, and R. T. Howie, *J. Chem. Phys.* **147**, 184303 (2017). 428
- 369 429
- 370 430
- 371 [28] C. Ji, A. F. Goncharov, V. Shukla, N. K. Jena, D. Popov, B. Li, J. Wang, Y. Meng, V. B. Prakapenka, J. S. Smith, R. Ahuja, W. Yang, and H.-k. Mao, *Proc. Natl. Acad. Sci. U.S.A.* **114**, 3596 (2017). 431
- 372 432
- 373 433
- 374 434
- 375 [29] D. Laniel, V. Svitlyk, G. Weck, and P. Loubeyre, *Phys. Chem. Chem. Phys.* **20**, 4050 (2018). 435
- 376 436
- 377 [30] R. Turnbull, M.-E. Donnelly, M. Wang, M. Peña-Alvarez, C. Ji, P. Dalladay-Simpson, H.-k. Mao, E. Gregoryanz, and R. T. Howie, *Phys. Rev. Lett.* **121**, 195702 (2018). 437
- 378 438
- 379 439
- 380 [31] J. Binns, P. Dalladay-Simpson, M. Wang, G. J. Ackland, E. Gregoryanz, and R. T. Howie, *Phys. Rev. B* **97**, 024111 (2018). 440
- 381 441
- 382 442
- 383 [32] M. Ceppatelli, D. Scelta, M. Serrano-Ruiz, K. Dziubek, G. Garbarino, J. Jacobs, M. Mezouar, R. Bini, and M. Peruzzini, *Nat. Commun.* **11**, 6125 (2020). 443
- 384 444
- 385 445
- 386 [33] W. L. Mao and H. K. Mao, *Proc. Natl. Acad. Sci. U.S.A.* **101**, 708 (2004). 446
- 387 447
- 388 [34] W. L. Mao, V. V. Struzhkin, H. K. Mao, and R. J. Hemley, *Chem. Phys. Lett.* **402**, 66 (2005). 448
- 389 449
- 390 [35] ~~Y. Liu, D. Duan, F. Tian, H. X. D. Li, Z. Zhao, X. Sha, B. Chu, H. Zhang, B. Liu, and T. Cui, RSC Adv. 4, 37569 (2014).~~ 450
- 391 451
- 392 [36] G. Saleh and A. R. Oganov, *Sci. Rep.* **6**, 32486 (2016). 452
- 393 453
- 394 [37] A. S. Naumova, S. V. Lepeshkin, and A. R. Oganov, *J. Phys. Chem. C* **123**, 20497 (2019). 454
- 395 455
- 396 [38] A. Zerr, G. Serghiou, R. Boehler, and M. Ross, *High Press. Res.* **26**, 23 (2006). 456
- 397 457
- 398 [39] H. Kadobayashi, S. Ohnishi, H. Ohfuji, Y. Yamamoto, M. Muraoka, S. Yoshida, N. Hirao, S. Kawaguchi-Imada, and H. Hirai, *Sci. Rep.* **11**, 8165 (2021). 458
- 399 459
- 400 [40] A. Kolesnikov, V. G. Kutcherov, and A. F. Goncharov, *Nat. Geosci.* **2**, 566 (2009). 460
- 401 461
- 402 [41] D. A. Kudryavtsev, ~~T. Fedotenko~~, E. G. Koemets, S. E. Khandarkhaeva, V. G. Kutcherov, and L. S. Dubrovinsky, *Sci. Rep.* **10**, 1483 (2020). 462
- 403 463
- 404 464
- 405 [42] E. Snider, N. Dasenbrock-Gammon, R. McBride, M. Debessai, H. Vindana, K. Vencatasamy, K. V. Lawler, A. Salamat, and R. P. Dias, *Nature (London)* **586**, 373 (2020). 465
- 406 466
- 407 467
- 408 [43] W. Cui, T. Bi, J. Shi, Y. Li, H. Liu, E. Zurek, and R. J. Hemley, *Phys. Rev. B* **101**, 134504 (2020). 468
- 409 469
- 410 [44] A. F. Goncharov, E. Bykova, M. Bykov, X. Zhang, Y. Wang, S. Chariton, and V. B. Prakapenka, *J. Appl. Phys.* **131**, 025902 (2022). 470
- 411 471
- 412 472
- [45] See Supplemental Material at <http://link.aps.org/supplemental/10.1103/PhysRevLett.000.000000> for further methodological details and additional experimental and computational figures, which includes Refs. [46–68]. 416
- [46] E. Aprà *et al.*, *J. Chem. Phys.* **152**, 184102 (2020). 417
- [47] S. B. Ramsey, M. Pena-Alvarez, and G. J. Ackland, *Phys. Rev. B* **101**, 214306 (2020). 418
- [48] V. Labet, R. Hoffmann, and N. W. Ashcroft, *J. Chem. Phys.* **136**, 074502 (2012). 419
- [49] V. Labet, R. Hoffmann, and N. W. Ashcroft, *J. Chem. Phys.* **136**, 074503 (2012). 420
- [50] H.-K. Mao, J. Xu, and P. M. Bell, *J. Geophys. Res.* **91**, 4673 (1986). 421
- [51] Y. Akahama and H. Kawamura, *J. Appl. Phys.* **100**, 043516 (2006). 422
- [52] Y. Grin, F. R. Wagner, M. Armbrüster, M. Kohout, A. Leithe-Jasper, U. Schwarz, U. Wedig, and H. G. von Schnering, *J. Solid State Chem.* **179**, 1707 (2006). 423
- [53] S. Schaack, U. Ranieri, P. Depondt, R. Gaal, W. F. Kuhs, P. Gillet, F. Finocchi, and L. E. Bove, *Proc. Natl. Acad. Sci. U.S.A.* **116**, 16204 (2019). 424
- [54] H. T. Stokes, D. M. Hatch, and B. J. Campbell, FINDSYM, ISOTROPY Software Suite ([iso.byu.edu](http://iso.byu.edu)). 425
- [55] H. T. Stokes and D. M. Hatch, *J. Appl. Crystallogr.* **38**, 237 (2005). 426
- [56] T. Ohba, Y. Kitano, and Y. Komura, *Acta Cryst. C* **40**, 1 (1984). 427
- [57] K. Ishizaki, P. Bolsaitis, and I. Spain, *Solid State Commun.* **15**, 1591 (1974). 428
- [58] J. J. Gilvarry, *Phys. Rev.* **102**, 308 (1956). 429
- [59] F. A. Lindemann, *Phys. Z.* **11**, 609 (1910). 430
- [60] K. Refson, P. R. Tulip, and S. J. Clark, *Phys. Rev. B* **73**, 155114 (2006). 431
- [61] A. Tkatchenko and M. Scheffler, *Phys. Rev. Lett.* **102**, 073005 (2009). 432
- [62] G. Gao, A. R. Oganov, Y. Ma, H. Wang, P. Li, Y. Li, T. Iitaka, and G. Zou, *J. Chem. Phys.* **133**, 1 (2010). 433
- [63] S. J. Clark, M. D. Segall, C. J. Pickard, P. J. Hasnip, M. I. J. Probert, K. Refson, and M. C. Payne, *Z. Krist.—Cryst. Mater.* **220**, 567 (2005). 434
- [64] K. Momma and F. Izumi, *J. Appl. Crystallogr.* **44**, 1272 (2011). 435
- [65] J. Gonzalez-Platas, M. Alvaro, F. Nestola, and R. Angel, *J. Appl. Crystallogr.* **49**, 1377 (2016). 436
- [66] J. Rodríguez-Carvajal, *Physica (Amsterdam)* **192B**, 55 (1993). 437
- [67] Y. Fei, A. Ricolleau, M. Frank, K. Mibe, G. Shen, and V. Prakapenka, *Proc. Natl. Acad. Sci. U.S.A.* **104**, 9182 (2007). 438
- [68] C. Prescher and V. B. Prakapenka, *High Press. Res.* **35**, 223 (2015). 439
- [69] P. Loubeyre, R. LeToullec, D. Hausermann, M. Hanfland, R. J. Hemley, H. K. Mao, and L. W. Finger, *Nature (London)* **383**, 702 (1996). 440
- [70] P. Loubeyre, R. Letoullec, and J. P. Pinceaux, *Phys. Rev. Lett.* **67**, 3271 (1991). 441
- [71] B. Chen, L. J. Conway, W. Sun, X. Kuang, C. Lu, and A. Hermann, *Phys. Rev. B* **103**, 035131 (2021). 442